

Fully Inkjet-Printed Green-Emitting PEDOT:PSS/NiO/Colloidal CsPbBr₃/SnO₂ Perovskite Light-Emitting Diode on Rigid and Flexible Substrates

Giovanni Vescio,* Gayathri Mathiazhagan,* Sergio González-Torres, Jesús Sanchez-Diaz, Alexis Villaeuva-Antolí, Rafael S. Sánchez, Andrés F. Gualdrón-Reyes, Marek Oszajca, Flavio Linardi, Alina Hauser, Felipe A. Vinocour-Pacheco, Wiktor Żuraw, Senol Öz, Sergi Hernández, Iván Mora-Seró,* Albert Cirera, and Blas Garrido

After establishing themselves as promising active materials in the field of solar cells, halide perovskites are currently being explored for fabrication of low-cost, easily processable, and highly efficient light-emitting diodes (LEDs). Despite this, the highest efficiencies reported for perovskite-based LEDs (PeLEDs) are achieved through spin coating or vacuum evaporation deposition techniques, which are not adequate, in most of the cases, for an industrial-scale production. Additionally, the long-term stability is still a big handicap, even though all inorganic perovskites, such as CsPbBr₃, are found to be more stable to external variables. In this context, herein, the fabrication of fully inkjet-printed (IJP) CsPbBr₃-based PeLEDs in ambient conditions, on rigid and flexible substrates, on a proof-of-concept basis, with the successful incorporation of NiO and SnO₂ as hole- and electron-selective contacts, respectively, is reported. Despite the moderate luminance (324 cd m⁻²) value obtained, this result paves the way toward the development of upscalable fabrication of PeLEDs based on deposition techniques with controlled spatial resolution.

the development of a new generation of solar cells, photodetectors, light-emitting diodes (LEDs), and color displays. The suitability of HPs for optoelectronic applications lies on their outstanding electro-optical properties, such as high photoluminescence quantum yield (PLQY),^[1] narrow photoluminescence full width at half maximum (FWHM), tunable bandgap, and high charge carrier mobility,^[2] among others. Perovskite-based LEDs (PeLEDs), which were first reported in the 1990s,^[3,4] have recently reached external quantum efficiencies (EQEs) that graze the maximum theoretical limits (EQE > 28%)^[5] with extremely high maximum luminance levels ($L_{\text{max}} = 470\,000 \text{ cd m}^{-2}$).^[5] Beyond EQE and luminance, the most severe drawback of PeLED technology is probably the limited long-term stability. Despite the

1. Introduction

In the last decade, halide perovskites (HPs) have been consolidated as an emerging family of promising materials for

latest improvements, their durability at operating conditions is still restricted to few hundreds of hours in the best cases, thus hampering its inclusion as a competitive lighting and/or display technology. The broadly reported instability of PeLEDs is

G. Vescio, G. Mathiazhagan, S. González-Torres, S. Hernández, A. Cirera, B. Garrido
MIND-IN2UB
Department of Electronics and Biomedical Engineering
Universitat de Barcelona
Martí i Franquès 1, 08028 Barcelona, Spain
E-mail: gvescio@ub.edu; gmathiazhagan@ub.edu

J. Sanchez-Diaz, A. Villaeuva-Antolí, R. S. Sánchez, A. F. Gualdrón-Reyes, I. Mora-Seró
Institute of Advanced Materials (INAM)
Universitat Jaume I (UJI)
Avenida de Vicent Sos Baynat, s/n, 12071 Castelló de la Plana, Spain
E-mail: sero@uji.es

M. Oszajca, F. Linardi, A. Hauser
Avantama AG
Laubisruetistrasse 50, Staefa 8712, Switzerland

F. A. Vinocour-Pacheco, W. Żuraw, S. Öz
Saule Research Institute
Dunska 11, 54-427 Wrocław, Poland

W. Żuraw
Department of Semiconductor Materials Engineering
Wrocław University of Science and Technology
Wybrzeże Wyspińskiego 27, 50-370 Wrocław, Poland

S. Öz
Solaveni GmbH
Siemensstraße 42, 59199 Bönen, Germany

 The ORCID identification number(s) for the author(s) of this article can be found under <https://doi.org/10.1002/adem.202300927>.

© 2023 The Authors. Advanced Engineering Materials published by Wiley-VCH GmbH. This is an open access article under the terms of the Creative Commons Attribution-NonCommercial License, which permits use, distribution and reproduction in any medium, provided the original work is properly cited and is not used for commercial purposes.

DOI: 10.1002/adem.202300927

generally associated with in situ generation of crystalline defects as a consequence of electroinduced ion migration mechanisms, that is, intrinsic degradation. Furthermore, the sensitivity of hybrid organic–inorganic HPs to external oxidizing agents and/or polar solvents, including moisture, compromises the long-term reliability of the devices.^[6–9] In this context, all-inorganic HPs, bearing cesium as A-site cation (CsPbBr₃), have shown better extrinsic stability levels compared to the hybrid organic–inorganic counterparts.^[6,10]

Besides the suitability of the light-active materials, the performance of LEDs strongly depends on the selective charge injection/transport layers,^[11,12] and apart from the purely electro-optical compatibility among the different stacked materials that constitute a PeLED, the device architecture and the deposition techniques/procedures used play a significant role not just on the ultimate performance of the devices, but in the final commercialization potential. In this context, reducing the organic layers, in both active and charge injecting layers, and the use of industrial friendly deposition technique seem to be the most convenient approach for the commercialization of PeLEDs. However, to the best of our knowledge, any example fulfilling the above-mentioned fabrication requirements can be found in the literature so far.

Poly(3,4-ethylenedioxythiophene):polystyrene sulfonate (PEDOT:PSS) is commonly used as a hole injection layer (HIL), due to its excellent electrical properties as an interfacial layer between transparent conductive oxides, for example, indium tin oxide (ITO), and the organic or inorganic materials deposited on top. Unfortunately, several studies suggest that the acidic and hygroscopic nature of PEDOT:PSS detrimentally affects the integrity of the HIL/halide perovskite (HP) interface in the long term, thus reducing the operational lifetime of devices.^[13,14] Therefore, other promising *p*-type semiconductors, such as carbon quantum dots (CQDs),^[15] copper sulfide gallium tin oxide (CuS–GaSnO),^[16] copper thiocyanate (CuSCN),^[17] vanadium oxide (V₂O₄),^[18] molybdenum oxide (MoO₃),^[19] poly(N,N'-bis(4-butylphenyl)-N,N'-bis(phenyl)-benzidine) (poly-TPD),^[20–23] or nickel oxide (NiO), have been successfully introduced between the PEDOT:PSS and the MHPs as hole-transporting materials (HTMs). Due to its outstanding stability in ambient conditions, high hole mobility, good charge injection properties, and lower trap density compared to other alternatives, NiO is an attractive choice to be exploited as HTM in PeLEDs.^[11–14,24,25] Interestingly, its high conduction band energy level (−1.8 eV) makes it an excellent electron blocking layer (EBL), able to confine the injected electrons into the MHP conduction band, thus minimizing electrical losses. Hence, *p*–*i*–*n* architecture is one of the most extended configurations to fabricate highly efficient PeLEDs.

Regarding the deposition techniques, most of the highly efficient PeLEDs reported so far are fabricated through spin coating, which allows the sequential deposition of the stacked materials.^[26] However, spin coating is not suitable for large-area fabrication, does not provide spatial resolution, and only ≈2% of the solution dropped contributes to the ultimate thin film.^[27] Among industrially relevant fabrication techniques, inkjet printing (IP) is one of the powerful upscalable techniques.^[28] Hermerschmidt et al. published the first inkjet-printed MAPbBr₃ PeLED whose maximum luminance was 4000 cd m^{−2} for devices based on PEDOT:PSS with different amounts of KCl as an additive to tune

the crystallization process of the HP.^[29] The same year, Sun and co-workers addressed the coffee stain effect by adding a poly(vinylpyrrolidone) (PVP) layer on top of the HIL to improve the crystallization dynamics of the inkjet-printed MHP layer and achieved an EQE of 9%.^[30] Even though the crystallization dynamics of the HPs deposited through IP is indeed different from those spin coated,^[31] our group also demonstrated very recently the fabrication of PeLEDs based on a tin perovskite (Sn-MHP) derivative deposited by IP,^[32] thus highlighting the appropriateness of this technique for the development of PeLEDs. Despite its feasibility and obvious interest, promoting an inkjet-printed defect-free HP layer from a precursor solution ink is still a big challenge.^[33] The IP of colloidal HP nanocrystals (HP-NCs) seems to be a more straightforward approach, despite its inherent complexity, to obtain high-quality thin-films. Nevertheless, it is worth pointing out that the design of inks to control the rheology of the solutions, that is, viscosity and surface tension, the concentration of HP-NCs or the use of additives, as well as the optimization of the printing parameters, are key factors to achieve highly luminescent, pinhole-free, and smooth layers suitable for the fabrication of IJP PeLEDs.^[33] Once the printability is reached, the following major challenge is to avoid the coffee ring effect that causes further inhomogeneity in the layers.^[34–36] Besides this, orthogonality of the selected solvents used in the underlying layer, for enhanced wettability, and in the incoming layer/s, to prevent degradation of the HP layer, determines the quality of the complete devices.

For all-inorganic perovskite NCs, a ternary solvent system using inkjet-compatible solvents such as naphthene, *n*–tridecane, and *n*–nonane was reported to yield PeLEDs with an EQE of 8.54%.^[34] On the contrary, a binary solvent combination was suggested to improve a FAPb_{0.7}Sn_{0.3}Br₃-based HP-NCs ink, which resulted in an EQE of 7.9%.^[37] Therefore, most of the improvement in inkjet-printed PeLEDs has been achieved through exploitation of passivation layers,^[30] by introducing additives^[29,38] and/or using cosolvents.^[27,34,35] It is worth noting that all the aforementioned precedents on IJP PeLEDs (except one, Table S1, Supporting Information) are based on the inkjet deposition of only the light-emitting layer, that is, MHP. Among them, only two works^[34,39] involved all-inorganic HP-NCs (CsPbBr₃). Interestingly, a fully IJP PeLED has been recently reported by Wang and co-workers, where a hybrid organic/inorganic HP was sandwiched between organic charge-selective contacts to reach a maximum EQE of 0.8%.^[40]

Thereby, we report in this work on the fabrication of fully inkjet-printed PeLEDs on rigid and flexible substrates, where not only the all-inorganic CsPbBr₃ NC ink but also the corresponding NiO and SnO₂ as charge-selective contacts have been printed, as a continuation of our previous study based on color conversion layers.^[35] To the best of our knowledge, this is the first proof of concept of a fully inkjet-printed PeLED where the light-active HP, CsPbBr₃-NCs, is sandwiched between inorganic charge-selective contacts completely deposited in ambient atmosphere.

2. Results and Discussion

In this section, the gradual evolution toward the fabrication of fully inkjet-printed PeLEDs based on an inorganic perovskite

is presented. A systematic characterization of fabricated PeLEDs is presented, where in all the cases an inkjet-printed CsPbBr₃ NC layer is used as the light-emissive layer. Progressively, IP deposition was applied to other relevant materials that constitute the devices, that is, HIL and EIL, respectively, until reaching a proof-of-concept fully inkjet-printed PeLED on both rigid (glass) and flexible substrates (PET).

2.1. Characterization of IJP NiO Layer

The NiO ink formulated by the company Avantama AG (details in the Experimental Section) showed required rheological printing properties with stable jetting dynamics. Inkjet-printed, pinhole-free, thin films of NiO were obtained on glass substrate to investigate its structural and morphological quality (Figure S1, Supporting Information). Postprocess thermal annealing of inkjet-printed NiO layers was performed in a vacuum oven (2 mbar) at 200 °C (details in Device Fabrication in Experimental section). The resultant IJP layer had a good morphology. The X-Ray diffraction (XRD) pattern in **Figure 1a** shows the characteristic peaks of NiO at 37.4° (111), 43.3° (200), 62.8° (220) corresponding to its cubic phase. Inset demonstrates the high transparency of IJP NiO layer on a glass substrate as corroborated by samples which present transmittance values >90% in the visible region, ensuring that IJP NiO contributes negligibly to any optical losses in the fully complete devices, see Figure S2 (Supporting Information). Additionally, the SEM image shown in Figure 1b confirms that the layer is smooth and pinhole free with an average particle size of 28–35 nm, confirming the aggregation of the nanoparticles (\approx 9 nm nanoparticle size in suspension reported for the ink) after the thermal post-treatment. For this purpose, we analyzed the device cross section by focused ion beam (FIB)-assisted field emission scanning electron microscopy (FESEM), as shown in Figure 1c. The section profile of the inkjet-printed NiO thin film shows homogeneity and integrity of the layer, with a thickness of around 75 nm. Besides compactness,

the cross section on the printed metal oxide does not show any propagation of printing errors or large cavities along the area. Additionally, electrical characterization of IJP NiO by Van der Pauw resistivity measurements showed that the conductivity is around 120 S cm⁻¹ (Figure S3, Supporting Information), which is comparable to that of films already reported values in the literature.^[41–43]

In order to ensure the expected electrical characteristics of the inkjet-printed charge injection layers, several p–n junctions were fabricated. Their electrical characterization results are demonstrated in Figure S4, Supporting Information, where all the measurements, for more than 30 devices, confirm that the all inkjet-printed PEDOT:PSS/NiO (HIL/HTM) stack showed the same electrical behavior as the single spin-coated PEDOT:PSS layer (SC PEDOT:PSS, Figure S5, Supporting Information).

2.2. First Step to Fully IJP PeLEDs: Optimization of IJP CsPbBr₃ Ink and IJP NiO as EBL

Following the successful evaluation of p–n junctions, CsPbBr₃ NCs were inkjet printed to fabricate PeLEDs. All device fabrication and characterization experiments were performed in ambient conditions after proper encapsulation, see Supporting Information. Preliminarily, the effect of the addition of IJP NiO as an EBL in the PeLED configuration was tested and compared to the single spin-coated layer PEDOT:PSS, as shown in **Figure 2a–c**, where the employed PeLED device architectures are presented in 3D structure, respectively. For all the analyzed devices in this section, the PEDOT:PSS layer was spin coated and the CsPbBr₃ NP was prepared through “Method 1” described under “Preparation of CsPbBr₃ colloidal solution” in the Experimental Section. The relevance and role of IJP NiO is presented with its corresponding band energy diagram shown in Figure 2b. The proposed band alignment suggests a smoother injection of holes to the CsPbBr₃ layer and the use of PEDOT:PSS allows an ohmic contact between with ITO,^[44] as ITO/NiO contact exhibits a non-Ohmic character. Additionally,

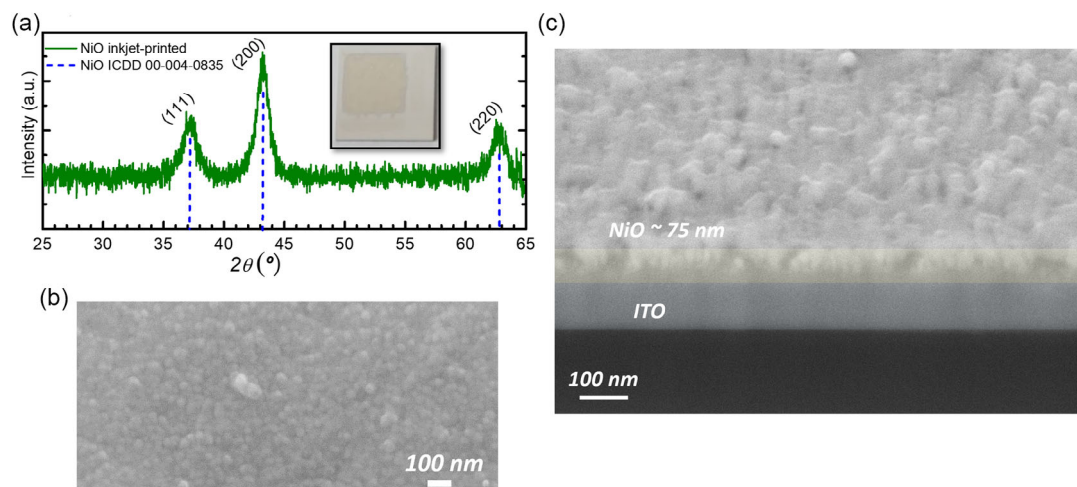


Figure 1. a) XRD pattern on IJP NiO showing characteristic peaks of cubic phase NiO. Inset shows the picture of a transparent IJP NiO film on glass substrate; b) top-view SEM image of IJP NiO; c) Cross section of the IJP NiO thin film by the FIB-assisted FESEM technique. The layers have an ITO bottom electrode thickness of 100 and 75 nm of NiO.

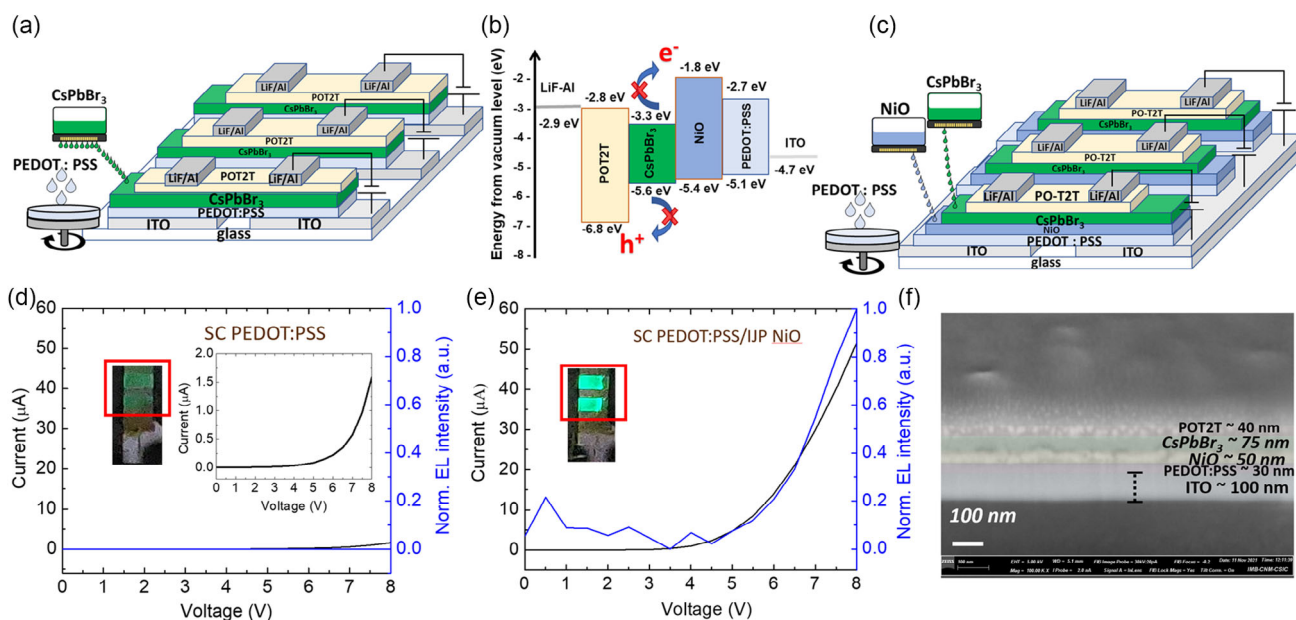


Figure 2. Results of complete PeLEDs with and without IJP NiO whose PEDOT:PSS was spin coated. a) 3D sketch of the fabricated PeLEDs with only spin-coated PEDOT:PSS layer as HIL for the complete corresponding device architectures. b) Energy band diagram for the proposed architecture.^[29,46,55–57] c) 3D sketch of the fabricated PeLEDs with the stack spin-coated PEDOT:PSS/inkjet-printed NiO layers as HIL and EBL materials for the complete corresponding device architectures. d) *I*–*V* curve at linear scale together with normalized EL intensity for devices with SC PEDOT:PSS as HIL. Insets contain a picture and a graph. The inset on the left corresponds to the picture of the emitting device at a bias voltage of 8 V. The inset on the right presents the detail with a zoom of the main graph showing the zoomed *I*–*V* curve with rescaled current range in the y-axis. e) *I*–*V* curve at linear scale together with normalized EL intensity for devices with SC PEDOT/IJP NiO as HIL and EBL. The related inset shows the image of the emitting device at a bias voltage of 8 V. The *I*–*V* curves correspond to the highlighted device in the image. Active area of these devices was 0.045 cm². f) FIB cross-section image of the proposed PeLED. The layers have a ITO bottom electrode, thickness of 100, 30 nm of SC PEDOT:PSS, 50 nm of IJP NiO, 75 nm of IJP CsPbBr₃, and 40 nm of evaporated POT2T.

IJP NiO acts as an excellent EBL as noticeable from the deep allowed level of conduction band energy. On the other side, POT2T is used as the reference electron injecting layer (EIL). See Experimental Section for details about the PeLED fabrication.^[45] Its energy band levels suggest an excellent hole blocking ability and good transfer of electrons to CsPbBr₃ layer.^[46] Figure S6, Supporting Information, shows the box plot of 6 devices from two criteria (i.e., SC PEDOT:PSS as HIL and a dual-layer stack of SC PEDOT/IJP NiO as EBL with their corresponding schematic representation in the inset). No significant differences were noticed in the average values of the current. Even though with the low observed currents, the comparison between the two proposed device architectures highlights the very low PeLEDs emission with only SC PEDOT:PSS layer (Figure 2d) and the undeniable role played by the introduction of IJP NiO. The measured *I*–*V* curves together with its normalized electroluminescence (EL) intensity prove that the IJP NiO is properly acting as the EBL enhancing the EL (Figure 2e), promoting a stronger emission of the pixels, compare inset in Figure 2d–e, although we do not observe current decreasing (details on insets in Figure S7, Supporting Information). These results confirm that we obtained, as far as we know, the first green-emitting CsPbBr₃ PeLEDs where the EBL is IJP NiO. The *I*–*V* electrical curves present the expected exponential behavior, confirming that these devices are free from Ohmic shunts. Moreover, by adding IJP NiO, a clear reduction of nonradiative recombination losses at

the perovskite interface has been obtained compared to the devices with simple structure of SC PEDOT/IJP CsPbBr₃. This may be due to the lower trap densities present in IJP NiO/perovskite interface as observed by Lee et al. and Wang et al.^[47,48] Figure 2f shows the FIB cross-section image of the proposed PeLED, with no evidence of structure anomalies (grains clustering) or defects generated (pinhole free) on the whole inkjet-printed PeLED structure.

Analyzing the origin of low intensity in the extracted luminosity from the achieved PeLEDs, it suggested that the synthesized CsPbBr₃ NCs through Method 1 contained ligands with insulating properties. This might have caused lower performances in the devices and resulted in faster degradation of PeLEDs under electrical stress. To demonstrate this hypothesis, an improved purification process of CsPbBr₃ NCs was employed to remove the undesirable ligands (see Method 2 in Experimental Section).

The improvement in the quality of CsPbBr₃ NCs was investigated using their IJP thin films as the active layer in a well-established PeLED architecture, whose HIL/EBL stack is completely spin coated, SC PEDOT/SC Poly TPD (best configuration reported so far in literature),^[49–51] and in the previously well-performed PeLED architecture with a dual-layer stack of SC PEDOT/IJP NiO. The results comparing these architectures shown in Figure S8, Supporting Information, display that similar maximum luminance and EQE are obtained for both the EBLs (i.e., SC Poly-TPD and IJP NiO). This fact points out that IJP NiO

is an efficient alternative inorganic EBL in the fabrication of PeLEDs. Moreover, a clear overall enhancement in the absolute value of luminance ($\approx 19\,000\text{ cd m}^{-2}$) of PeLEDs is obtained with SC PEDOT/IJP NiO, which is attributed to the new improved inkjet-printed CsPbBr₃ NC-based ink (by Method 2, Synthesis). Herewith, the PeLEDs prepared hereafter use the perovskite ink containing improved CsPbBr₃ NC washing.

2.3. Second Step to Fully IJP PeLEDs: IJP PEDOT:PSS Layer

After the study of the positive effect of addition of IJP NiO as the EBL and its interface matching with the improved CsPbBr₃ NC thin films, the next step toward fully IJP PeLEDs analyzed the effect of the deposition method of PEDOT:PSS HIL comparing between spin-coating and inkjet printing technology. Here also, POT2T was maintained as the EIL layer was fabricated through vacuum evaporation. **Figure 3a,b** shows the different device architectures fabricated in this section on rigid and flexible PET substrates (details in the Experimental Section). Both proposed PeLED device structures reached comparable stable high current densities (Figure 3c). However, measuring the luminance as a function of the operating voltage, the devices with the fully printed stack IJP PEDOT:PSS/IJP NiO PeLEDs presented a decrease in brightness with a maximum value of 1639 cd m^{-2} (Figure 3d), which is a promising result (one order below $19\,230\text{ cd m}^{-2}$ for SC PEDOT:PSS devices), considering that any difference was appreciated between the rigid and flexible substrates. These values confirm that the presented LED device structures reached competitive and comparable performance to the previous best values reported in the literature for IJP PeLEDs

based on CsPbBr₃ NCs. On the other hand, much effort is required in terms of the efficiency as estimated by the EQE measurements, plotted as a function of voltage (Figure 3d). It can be estimated that the undesired nonradiative charge recombination for IJP LEDs is probably due to the higher roughness of IJP PEDOT:PSS at the interfaces with ITO and NiO, respectively. The main reason could be associated with the fast solvent evaporation of the used commercial PEDOT:PSS ink (best conductivity value in the market, $\approx 1000\text{ S cm}^{-1}$) during the printing process. Notably, the PL spectra measured for all devices show a narrow curve whose FWHM was $\approx 21\text{ nm}$ (Figure S9, Supporting Information), confirming that the PL was not influenced by the nature of the HIL layers. In addition, the turn-on voltage is around 3.0 V in both proposed configurations with a maximum EQE of 2.5% reached for SC PEDOT:PSS PeLEDs, whereas for devices with IJP PEDOT:PSS, efficiencies were around 0.38% , which is one order of magnitude lower, as observed for the luminance absolute values. Finally, we confirmed that moving the fabrication of LED devices from rigid to flexible substrate did not promote any decrease of performances. Similarly, EQE, plotted as a function of voltage, verifies the tendency.

2.4. Third Step to Fully IJP PeLEDs: IJP SnO₂ as EIL

Once the feasibility of inkjet printing technology for the fabrication of competitive green-emitting PeLEDs was demonstrated, not only the emissive active layer but also the EILs were inkjet printed as a proof of concept of a fully inkjet-printed PeLEDs. Vacuum-evaporated organic POT2T EIL is replaced by the inorganic IJP SnO₂, which could ensure high electronic conductivity

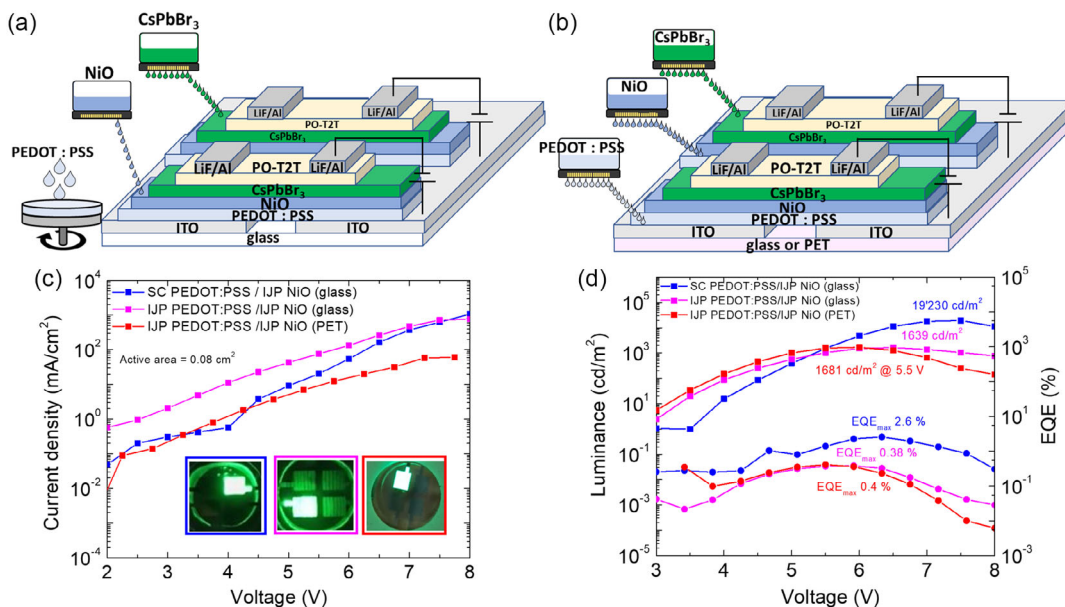


Figure 3. Results of PeLED devices comparing SC PEDOT:PSS and IJP PEDOT:PSS as HTL and POT2T as ETL are shown. a) Schematic structure of PeLEDs with the spin-coated PEDOT:PSS/inkjet-printed NiO layers as HTL and EBL materials for the complete corresponding device architectures. b) 3D sketch of the fabricated PeLEDs with the HIL/EBL stack fully printed. c) Current density versus voltage characteristic, insets show the images of the green-emitting rigid (squared blue and pink lines) and flexible (red squared line) LEDs operating at 7 V. d) Luminance and EQE versus voltage characteristics. The active area of each device is 0.08 cm^2 .

(mobility of $250 \text{ cm}^2 \text{ V}^{-1} \text{ s}^{-1}$), wide bandgap (3.8 eV), less hygroscopic property in nature, UV stability, and excellent optical transparency. Having similar energy band levels to POT2T, SnO_2 also act as an effective hole blocking layer. Solution deposition on the perovskite layer, especially in ambient conditions, is a challenge. Indeed, to achieve successful emission in an all-inkjet-printed device, the orthogonality of the solvents at the interfaces plays an important role. Here an inkjet-printable SnO_2 ink, developed by Avantama AG company, was employed. Investigations on standalone IJP SnO_2 on glass resulted in smooth, pinhole-free, and transparent SnO_2 layers with expected crystalline and structural properties (see Figure S10, Supporting Information). The effect of the addition of IJP SnO_2 as an EIL in the PeLED configuration, as shown in Figure 4, was verified by the comparison between the device with SC PEDOT:PSS layer as HIL and the fully inkjet-printed PeLEDs on both, rigid and flexible substrates. Figure 4a,c shows the 3D pictorial representation of the proposed device architectures, highlighting their difference in fabrication processes, with their correlated energy band diagram (Figure 4b).

The carried out current density and luminance as a function of the operating voltage on glass substrates demonstrated the similarity among the two proposed structure, establishing solution-processable inkjet printing technology as a feasible method for the fabrication of PeLEDs (Figure 4d). Analyzing in depth the results, comparing the I - V curve characteristics,

both devices present same tendency and behavior with a turn-on voltage around 3 V, where the fully-printed PeLEDs reached lower values in terms of absolute maximum luminance (324 cd m^{-2}) and efficiency (EQE of 0.017%, Figure S11d, Supporting Information). Moreover, the EL spectral characteristics showed that all the fabricated PeLEDs emitted a pure green with a peak centered at 517 nm and FWHM of 22 nm (see Figure S11b, Supporting Information), as previously observed in the devices with evaporated POT2T, thus proving the good quality of the fully printed $\text{CsPbBr}_3/\text{SnO}_2$ interface. Moving the fabrication of LED devices from the rigid to flexible substrate promotes a slight decrease of performances, probably due to the encapsulation and postprocesses (Figure 4e).

Device stability was studied in ambient conditions under continuous electrical stress to set an initial luminance of 100 cd m^{-2} . The stability monitoring over time determined the figure of merit known as t_{50} , the time in which EL decays to the 50% of its initial value. The accelerated loss of performance, $t_{50} \approx 2$ –3 min (Figure S11d, Supporting Information), of the fully printed devices emphasized that stability is still a main remaining milestone to achieve for large-scale fabrication by solution processing methods like inkjet printing technology. The presented devices correspond, to the best of our knowledge, to the first demonstration of the feasibility of fully inkjet-printed inorganic green-emitting CsPbBr_3 NCs-based PeLEDs, where PEDOT:PSS/NiO and SnO_2 are deposited as

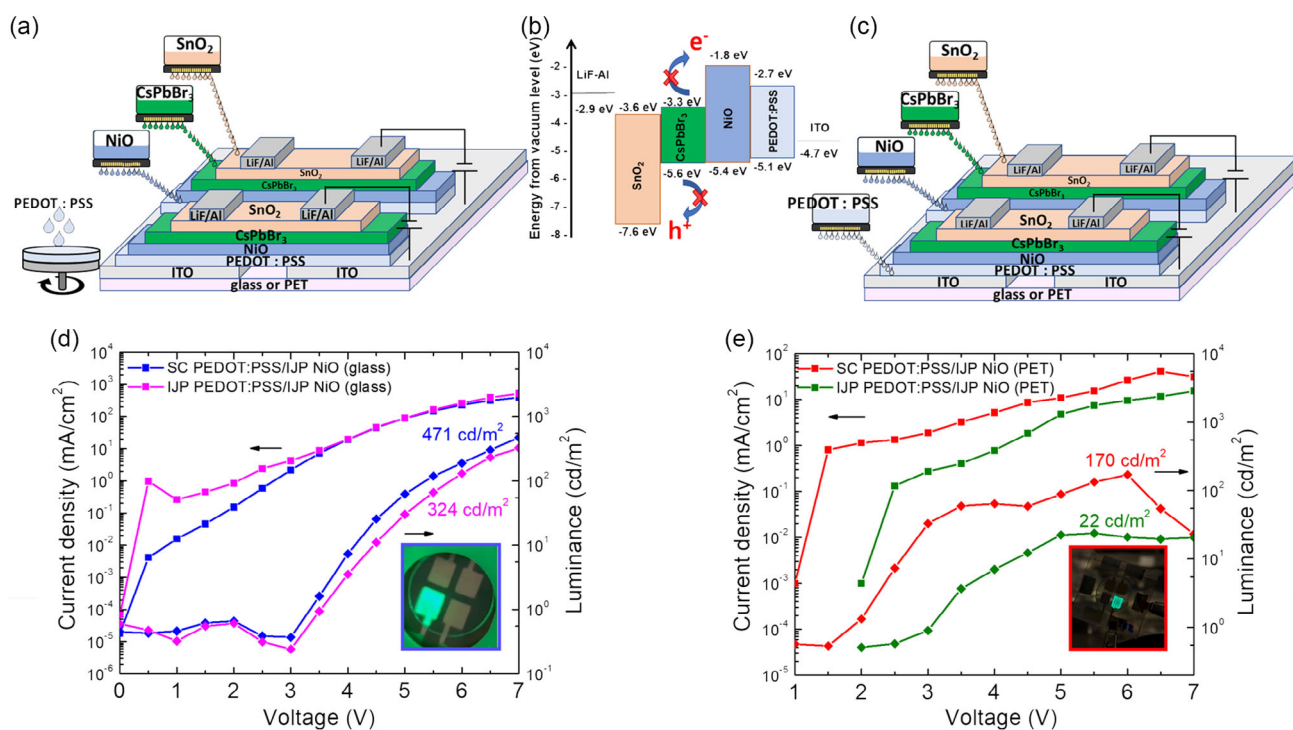


Figure 4. Results of PeLEDs with IJP SnO_2 as electron transport material (ETM). Comparison of devices having SC PEDOT:PSS and IJP PEDOT:PSS is shown. a) 3D sketch of the fabricated PeLEDs fully printed where only spin-coated PEDOT:PSS layer as HIL is used for the complete corresponding device architectures. b) Energy band diagram for the proposed architecture.^[29,46,55–57] c) 3D sketch of the fully inkjet printed-fabricated PeLEDs. d) Current density and luminance versus voltage characteristic of compared device structures on glass substrate, inset shows the images of the green-emitting LEDs operating at 6 V. e) Current density and luminance versus voltage characteristic of compared device structures on flexible PET substrate, inset shows the images of the green-emitting LEDs operating at 6 V. The active area of the devices is 0.08 cm^2 .

HIL/EBL and EIL, respectively, on both rigid and flexible substrates. The potential exploitation of this technique with the wide range of inorganic materials ensures future scalability in area and number of devices for mass production required in industry.

3. Conclusion

In this work, we report, to the best of our knowledge, the first fully inkjet-printed PeLEDs sandwiched between inorganics metal oxide charge transport layers on both rigid and flexible substrates. This proof-of-concept system is based on the printing of colloidal CsPbBr₃ NCs as a light-emitting layer, whereas PEDOT:PSS, NiO, and SnO₂ inks, respectively, are used as charge-selective contacts. We demonstrate that, regardless of the PEDOT:PSS deposition method (spin coating or inkjet printing), the addition of IJP NiO as EBL enhances the PeLED performance. Despite the reduced performance of a fully inkjet-printed PeLED, on both rigid and flexible substrates, this work highlights, on the one hand, the possibility to fully fabricate an inorganic PeLED using industry-friendly inkjet printing technique and on the other hand, the need to further optimize the charge injection and blocking layer, that have received significantly less attention in the development of PeLEDs. These promising results pave the way for ambient-processed all-inorganic fully inkjet-printed PeLEDs for broad optoelectronic applications.

4. Experimental Section

Method 1: The CsPbBr₃ NCs were synthesized by following the hot injection method described by Kovalenko and co-workers^[26,52] with some modifications.^[53] All the reactants were used as received without any additional purification process. To prepare a Cs-oleate solution, 0.41 g of Cs₂CO₃ (Sigma-Aldrich, 99.9%), 1.5 mL of oleic acid (OA, Sigma-Aldrich, 90%), and 20 mL of 1-octadecene (1-ODE, Sigma-Aldrich, 90%) were loaded together into a 50 mL three-necked flask and degassed at 120 °C in vacuum for 1 h under constant stirring. Then, the mixture was N₂ purged and heated to 150 °C until the complete dissolution of the Cs₂CO₃. The solution was stored under N₂, keeping the temperature at 120 °C. Second, 0.85 g of PbBr₂ (ABCR, 99.999%) was mixed with 50 mL of 1-ODE into a 100 mL three-necked flask. The mixture was heated at 120 °C in vacuum for 1 h with constant stirring. Then, 10 mL of a pre-heated mixture (130 °C) of OA and oleylamine (OLA, Sigma-Aldrich, 98%) 1:1 in volume were added to the flask under N₂, and the mixture was quickly heated to 170 °C. Simultaneously, 4 mL of Cs-oleate solution was swiftly added to the mixture. After 5 s of reaction, the flask was immersed into an ice bath to quench the reaction. To purify the NCs, 60 mL of methyl acetate (99.5%, Sigma-Aldrich) were added to 30 mL of liquor solution, and the colloidal solution was centrifuged at 5000 rpm for 10 min. Then, NC precipitate was separated after discarding the supernatant. Two solutions were prepared by redispersing them in dodecane and hexane separately to concentrate the NCs at 50 mg mL⁻¹.

Method 2: In this method, the synthesis of CsPbBr₃ NCs was similar to Method 1; however, a different purification process was carried out. Cesium carbonate (Cs₂CO₃, 0.407 g, 1.25 mmol) and oleic acid (OA, 1.25 mL, 3.5 mmol) were loaded into a 50 mL three-necked flask with octadecene (ODE, 20 mL) and heated at 120 °C under for 1 h in vacuum. Then, the flask atmosphere was refilled with nitrogen and the temperature of the mixture was increased to 150 °C until the complete dissolution of cesium carbonate. Separately, a 100 mL three-necked flask was loaded with lead bromide (PbBr₂, 0.345 g, 0.94 mmol), oleic acid (OA, 2.5 mL, 7.1 mmol), and oleylamine (OLEA, 2.5 mL, 5.3 mmol) with octadecene (ODE, 25 mL).

The mixture was dried for 1 h at 120 °C in vacuum. Then, the temperature was increased to 170 °C under N₂ atmosphere and 2 mL of cesium oleate solution was swiftly injected and after 5 s, the flask was immersed into an ice water bath to stop the reaction. The crude was centrifuged (5000 rpm, 5 min); the supernatant was discarded, and the precipitate was dispersed in hexane (5 mL). Then, MeOAc (5 mL) was added to the dispersion and second centrifugation was carried out (5000 rpm, 5 min); again, the supernatant was discarded, and the solid was redispersed in hexane (1 mL). At this point, the dispersion was stored in an Eppendorf vial at low temperature (−18 °C) overnight and carefully decanted to remove the solid sediment deposited at the bottom. Then, the dispersion was transferred to a glass vial, dried with a gentle nitrogen flow, and introduced in vacuum for 15 min to obtain the CsPbBr₃ nanoparticles as a solid. Finally, the solid was weighed (60–70 mg was typically obtained), redispersed in the corresponding volume of hexane or dodecane (typically 6–7 mL) to obtain a concentration of 10 mg mL⁻¹, and filtered through a 0.42 μm Teflon filter for device's fabrication.^[54]

Preparation of Inkjet-Printable Inks Based on CsPbBr₃ Nanocrystals: Two colloidal solution of CsPbBr₃ NCs in dodecane and CsPbBr₃ NCs in hexane (both prepared selecting the proper aforementioned methods) were mixed (ratio of dodecane/hexane 3:1), preserving the NC final concentration in the solution to be around 10% in weight.^[35] The obtained colloidal solution was stirred at room temperature and the supernatant was collected. The filtered solution of perovskite NC ink was then used for inkjet printing of the active layer of the PeLEDs reported in this article.

Device Fabrication: The first step in cleaning was to remove unwanted particle and residues to prepare the substrates for device manufacturing. ITO-patterned glass substrates were first ultrasonically cleaned using a 3% Hellmanex soap solution for 5 min. Further cleaning was done using deionized (DI) water, acetone, and isopropanol respectively in an ultrasonic bath each for 5 min. N₂ gun was used to dry the substrates. Poly(3,4-ethylenedioxythiophene):poly(styrenesulfonate) PEDOT:PSS (AL 4083 from Heraeus) solution was commercially bought from Alfa Aesar. Before spin coating, this solution was filtered using 0.22 μm cellulose acetate (CA) filter and then ultrasonicated for 20 min. Additionally, the glass substrates were treated with UV ozone (UVO) for 15 min to reduce its surface tension. 100 μL of PEDOT:PSS was dropped on the treated glass substrates. It was spin coated at 3000 rpm for 30 s. For inkjet printing, a Dimatix printer (Fujifilm Dimatix Inc.) with a cartridge of 21 μm diameter nozzle was used. Hence, for IJP PEDOT, a drop spacing of 40 μm was used. The substrate temperature was maintained at 50 °C for proper adhesion. Irrespective of their deposition method, PEDOT was annealed at 150 °C for 15 min. NiO (2.5 wt% of NiO nanoparticle dispersion in hexanol from Avantama AG) was then inkjet printed with a drop spacing of 70 μm and annealed at 150 °C for 30 min in a vacuum oven at 65 mbar. Subsequently, CsPbBr₃ was inkjet printed using the formulation from Method 1^[35] or Method 2 (as mentioned in the earlier section). Two layers of CsPbBr₃ were inkjet printed at a drop spacing of 40 μm where the substrate temperature was maintained at 45 °C. Perovskite layer was then annealed at 95 °C for 10 min. For processing the electron injection layer (EIL), the devices with IJP CsPbBr₃ were transferred to the vacuum evaporator. 30 nm of 2,4,6-tris[3-(diphenylphosphinyl)phenyl]-1,3,5-triazine (POT2T from Lumtec) was deposited. In case of SnO₂ as the EIL, the inks were acquired from Avantama AG (SnO₂ nanoparticles dispersed in hexanol 2.5% in weight). They were inkjet printed with 40 μm drop spacing and annealed in a vacuum oven at 95 °C for 10 min. Finally, 1 nm LiF (Sigma Aldrich) and 150 nm Al (Lesker, 99.99% pellets) respectively were vacuum evaporated as electrodes to complete the device fabrication.^[45] All the layers before vacuum evaporation were carried out in the ambient atmosphere, an advantage with regard to other inkjet-printed perovskite materials. All the data for PeLED devices characterization were acquired after encapsulation. A photocurable glue (Lumtec LT-U001) and a glass slide cover (Thermo scientific MENZBC080080A120) were used to encapsulate the active area with 4 min exposure to UV light.

Characterization of PeLEDs: For the EL measurements with the proposed CsPbBr₃ NCs-based ink Method-1, an Ossila (S211) system together with its corresponding software was used to collect and consolidate the data. Then with the improvement to the CsPbBr₃ NCs-based ink

Method-2, the complete EL characterization was carried out by a Hamamatsu C9920-12 EQE measurement system, which allows to acquire the data at various voltages. To measure the EL intensity, a GAMRY Reference 3000 potentiostat coupled with a charge coupled device (CCD) detector (Andor-iDUS DV420A-OE) and a spectrograph (Kymera 1931-B2) was used. Scanning electron microscope (SEM) images were acquired using the FEGSEM – JEOL 3100F system. Transmittance, reflectance, and correlated absorbance spectra of metal oxides were registered using an integrating sphere (Bentham PV300 EQE system) with a Xe and quartz halogen dual-lamp source to measure between 300 and 1100 nm wavelength. The optical signals were captured by InGaAs photodetector.

Supporting Information

Supporting Information is available from the Wiley Online Library or from the author.

Acknowledgements

The authors wish to thank the financial support from the European Commission via FET Open Grant (862656, DROP-IT), MINECO (Spain) for grant PID2019-105658RB-I00 (PRITES project), Ministry of Science and Innovation of Spain under Project STABLE (PID2019-107314RB-I00), and Generalitat Valenciana via Prometeo Grant Q-Devices (Prometeo/2018/098).

Conflict of Interest

The authors declare no conflict of interest.

Data Availability Statement

The data that support the findings of this study are available from the corresponding author upon reasonable request.

Keywords

CsPbBr₃, green emission, inkjet printing, light-emitting diodes, metal oxides, nanocrystals, perovskites

Received: July 17, 2023

Published online:

- [1] A. F. Gualdrón-Reyes, S. Masi, I. Mora-Seró, *Trends Chem.* **2021**, *3*, 499.
- [2] A. K. Jena, A. Kulkarni, T. Miyasaka, *Chem. Rev.* **2019**, *119*, 3036.
- [3] M. Era, S. Morimoto, T. Tsutsui, S. Saito, *Appl. Phys. Lett.* **1994**, *65*, 676.
- [4] K. Chondroudis, D. B. Mitzi, *Chem. Mater.* **1999**, *11*, 3028.
- [5] J. S. Kim, J.-M. Heo, G.-S. Park, S.-J. Woo, C. Cho, H. J. Yun, D.-H. Kim, J. Park, S.-C. Lee, S.-H. Park, E. Yoon, N. C. Greenham, T.-W. Lee, *Nature* **2022**, *611*, 688.
- [6] Y. Hu, Q. Wang, Y. L. Shi, M. Li, L. Zhang, Z. K. Wang, L. S. Liao, *J. Mater. Chem. C* **2017**, *5*, 8144.
- [7] Y. Chen, M. He, J. Peng, Y. Sun, Z. Liang, *Adv. Sc.* **2016**, *3*, 1500392.
- [8] J. A. McLeod, L. Liu, *J. Phys. Chem. Lett.* **2018**, *9*, 2411.
- [9] Y. Han, S. Meyer, Y. Dkhissi, K. Weber, J. M. Pringle, U. Bach, L. Spiccia, Y.-B. Cheng, *J. Mater. Chem. A* **2015**, *3*, 8139.

- [10] J. Liang, C. Wang, P. Zhao, Z. Lu, Y. Ma, Z. Xu, Y. Wang, H. Zhu, Y. Hu, G. Zhu, L. Ma, T. Chen, Z. Tie, J. Liu, Z. Jin, *Nanoscale* **2017**, *9*, 11841.
- [11] W. Zheng, Q. Wan, Q. Zhang, M. Liu, C. Zhang, B. Wang, L. Kong, L. Li, *Nanoscale* **2020**, *12*, 8711.
- [12] S. Zhuang, J. He, X. Ma, Y. Zhao, H. Wang, B. Zhang, *Mater. Sci. Semicond. Process* **2020**, *109*, 104924.
- [13] S. Lee, D. Bin Kim, I. Hamilton, M. Daboczi, Y. S. Nam, B. R. Lee, B. Zhao, C. H. Jang, R. H. Friend, J. S. Kim, M. H. Song, *Adv. Sc.* **2018**, *5*, 1801350.
- [14] H. Wang, H. Yuan, J. Yu, C. Zhang, K. Li, M. You, W. Li, J. Shao, J. Wei, X. Zhang, R. Chen, X. Yang, W. Zhao, *ACS Appl. Mater. Interfaces* **2020**, *12*, 53528.
- [15] Z. Wang, F. Yuan, W. Sun, H. Shi, T. Hayat, A. Alsaedi, L. Fan, Z. Tan, *Adv. Opt. Mater.* **2019**, *7*, 1901299.
- [16] A. R. B. M. Yusoff, A. E. X. Gavim, A. G. Macedo, W. J. da Silva, F. K. Schneider, M. A. M. Teridi, *Mater. Today Chem.* **2018**, *10*, 104.
- [17] N. Arora, M. I. Dar, A. Hinderhofer, N. Pellet, F. Schreiber, S. M. Zakeeruddin, M. Grätzel, *Science* **2017**, *358*, 768.
- [18] H. Sun, X. Hou, Q. Wei, H. Liu, K. Yang, W. Wang, Q. An, Y. Rong, *Chem. Commun.* **2016**, *52*, 8099.
- [19] L. Zhang, X. Yang, Q. Jiang, P. Wang, Z. Yin, X. Zhang, H. Tan, Y. Yang, M. Wei, B. R. Sutherland, E. H. Sargent, J. You, *Nat. Commun.* **2017**, *8*, 15640.
- [20] D. Luo, Q. Chen, Y. Qiu, M. Zhang, B. Liu, *Nanomaterials* **2019**, *9*, 1007.
- [21] X. Zhang, H. Lin, H. Huang, C. Reckmeier, Y. Zhang, W. C. H. Choy, A. L. Rogach, *Nano Lett.* **2016**, *16*, 1415.
- [22] J. Li, L. Xu, T. Wang, J. Song, J. Chen, J. Xue, Y. Dong, B. Cai, Q. Shan, B. Han, H. Zeng, *Adv. Mater.* **2017**, *29*, 1603885.
- [23] T. Chiba, K. Hoshi, Y.-J. Pu, Y. Takeda, Y. Hayashi, S. Ohisa, S. Kawata, J. Kido, *ACS Appl. Mater. Interfaces* **2017**, *9*, 18054.
- [24] S. Zhuang, X. Ma, D. Hu, X. Dong, B. Zhang, *Ceram. Int.* **2018**, *44*, 4685.
- [25] P. Du, J. Li, L. Wang, L. Sun, X. Wang, X. Xu, L. Yang, J. Pang, W. Liang, J. Luo, Y. Ma, J. Tang, *Nat. Commun.* **2021**, *12*, 4751.
- [26] L. Protesescu, S. Yakunin, M. I. Bodnarchuk, F. Krieg, R. Caputo, C. H. Hendon, R. X. Yang, A. Walsh, M. V. Kovalenko, *Nano Lett.* **2015**, *15*, 3692.
- [27] T. Ye, S. Jia, Z. Wang, R. Cai, H. Yang, F. Zhao, Y. Tan, X. Sun, D. Wu, K. Wang, *Micromachines* **2022**, *13*, 983.
- [28] M. Singh, H. M. Haverinen, P. Dhagat, G. E. Jabbour, *Adv. Mater.* **2010**, *22*, 673.
- [29] F. Hermerschmidt, F. Mathies, V. R. F. Schröder, C. Rehmann, N. Z. Morales, E. L. Unger, E. J. W. List-Kratochvil, *Mater. Horiz.* **2020**, *7*, 1773.
- [30] Y. Li, Z. Chen, D. Liang, J. Zang, Z. Song, L. Cai, Y. Zou, X. Wang, Y. Wang, P. Li, X. Gao, Z. Ma, X. Mu, A. El-Shaar, L. Xie, W. Su, T. Song, B. Sun, *Adv. Opt. Mater.* **2021**, *9*, 2100553.
- [31] Y. Cheng, H. Wu, J. Ma, P. Li, Z. Gu, S. Zang, L. Han, Y. Zhang, Y. Song, *CCS Chem.* **2022**, *4*, 1465.
- [32] G. Vescio, J. Sanchez-Diaz, J. L. Frieiro, R. S. Sánchez, S. Hernández, A. Cirera, I. Mora-Seró, B. Garrido, *ACS Energy Lett.* **2022**, *7*, 3653.
- [33] P. Maisch, K. C. Tam, D. Jang, M. Steinberger, F. Yang, C. J. Brabec, H.-J. Egelhaaf, in *Organic Flexible Electronics, Fundamentals, Devices, and Applications Woodhead Publishing Series in Electronic and Optical Materials Elsevier* **2021**, pp. 305–333.
- [34] C. Wei, W. Su, J. Li, B. Xu, Q. Shan, Y. Wu, F. Zhang, M. Luo, H. Xiang, Z. Cui, H. Zeng, *Adv. Mater.* **2022**, *34*, 2107798.
- [35] G. Vescio, J. L. Frieiro, A. F. Gualdrón-Reyes, S. Hernández, I. Mora-Seró, B. Garrido, A. Cirera, *Adv. Mater. Technol.* **2022**, *7*, 2101525.

- [36] F. Mathies, E. J. W. List-Kratochvil, E. L. Unger, *Energy Technol.* **2020**, *8*, 1900991.
- [37] T. Ye, S. Jia, Z. Wang, R. Cai, H. Yang, F. Zhao, Y. Tan, X. Sun, D. Wu, K. Wang, *Micromachines* **2022**, *13*, 983.
- [38] V. R. F. Schröder, N. Fratzscher, F. Mathies, E. R. Nandayapa, F. Hermerschmidt, E. L. Unger, E. J. W. List-Kratochvil, *Nanoscale* **2023**, 5649.
- [39] C. Zheng, X. Zheng, C. Feng, S. Ju, Z. Xu, Y. Ye, T. Guo, F. Li, *Org. Electron.* **2021**, *93*, 106168.
- [40] J. Zhao, L. Lo, H. Wan, P. Mao, Z. Yu, C. Wang, *Adv. Mater.* **2021**, *33*, 2102095.
- [41] T. Ivanova, A. Harizanova, M. Shipochka, P. Vitanov, *Materials* **2022**, *15*, 1742.
- [42] M. Jlassi, I. Sta, M. Hajji, H. Ezzaouia, *Mater. Sci. Semicond. Process.* **2014**, *21*, 7.
- [43] F. Menchini, M. L. Grilli, T. Dikonimos, A. Mittiga, L. Serenelli, E. Salza, R. Chierchia, M. Tucci, *Phys. Status Solidi C* **2016**, *13*, 1006.
- [44] S.-M. Pan, R.-C. Tu, Y.-M. Fan, R.-C. Yeh, J.-T. Hsu, *IEEE Photonics Technol. Lett.* **2003**, *15*, 646.
- [45] K. M. M. Salim, E. Hassanabadi, S. Masi, A. F. Gualdrón-Reyes, M. Franckevicius, A. Devižis, V. Gulbinas, A. Fakharuddin, I. Mora-Seró, *ACS Appl. Electron. Mater.* **2020**, *2*, 2525.
- [46] J.-H. Lee, S.-H. Cheng, S.-J. Yoo, H. Shin, J.-H. Chang, C.-I. Wu, K.-T. Wong, J.-J. Kim, *Adv. Funct. Mater.* **2015**, *25*, 361.
- [47] S. Y. Lee, S. H. Jang, G. Lee, N. Park, J. Park, D. H. Park, K. H. Cho, J. W. Jung, J. Choi, *Ultrason. Sonochem.* **2022**, *89*, 106145.
- [48] Z. Wang, Z. Luo, C. Zhao, Q. Guo, Y. Wang, F. Wang, X. Bian, A. Alsaedi, T. Hayat, Z. Tan, *J. Phys. Chem. C* **2017**, *121*, 28132.
- [49] M. H. Tremblay, K. Schutt, Y. Zhang, J. Lim, Y. H. Lin, J. H. Warby, S. Barlow, H. J. Snaith, S. R. Marder, *Sustainable Energy Fuels* **2019**, *4*, 190.
- [50] E. Akman, S. Akin, *Adv. Mater.* **2021**, *33*, 2006087.
- [51] J. Höcker, D. Kiermasch, P. Rieder, K. Tvingstedt, A. Baumann, V. Dyakonov, *Z. Naturforsch. A* **2019**, *74*, 665.
- [52] J. Navarro-Arenas, I. Suárez, V. S. Chirvony, A. F. Gualdrón-Reyes, I. Mora-Seró, J. Martínez-Pastor, *J. Phys. Chem. Lett.* **2019**, *10*, 6389.
- [53] E. Hassanabadi, M. Latif, A. F. Gualdrón-Reyes, S. Masi, S. J. Yoon, M. Poyatos, B. Julián-López, I. Mora-Seró, *Nanoscale* **2020**, *12*, 14194.
- [54] R. S. Sánchez, A. Villanueva-Antolí, A. Bou, M. Ruiz-Murillo, I. Mora-Seró, J. Bisquert, *Adv. Mater.* **2022**, *35*, 2207993.
- [55] C.-Y. Huang, S.-P. Chang, A. G. Ansay, Z.-H. Wang, C.-C. Yang, *Coatings* **2020**, *10*, 336.
- [56] S. Ahn, K. Yabumoto, Y. Jeong, K. Akagi, *Polym. Chem.* **2014**, *5*, 6977.
- [57] A. Turak, *Electron. Mater.* **2021**, *2*, 198.